Letter Vol. 5, No. 12 / December 2018 / Optica 1603

optica

Self-phase modulation cancellation in a high-power ultrafast thin-disk laser oscillator

F. Saltarelli,* A. Diebold, I. J. Graumann, C. R. Phillips, and U. Keller

Institute for Quantum Electronics, ETH Zurich, 8093 Zurich, Switzerland
**Corresponding author: saltarelli@phys.ethz.ch*

Received 18 July 2018; revised 5 November 2018; accepted 15 November 2018 (Doc. ID 338780); published 11 December 2018

Ultrafast high-power lasers are employed in a wide variety of applications in science and industry. Thin-disk oscillators can offer compelling performance for these applications. However, because of the high intracavity peak power, a large amount of self-phase modulation (SPM) is picked up in the intracavity air environment. Consequently, the highest performance oscillators have been operated in a vacuum environment. Here, we introduce a new concept to overcome this hurdle. We cancel the SPM picked up in air by introducing an intracavity phase-mismatched second-harmonic-generation crystal. The resulting cascaded $\chi^{(2)}$ processes provide a large SPM with a sign opposite the one originating from the air. This enables laser operation in air at 210 W average output power with 780 fs, 19 μJ pulses, the highest output power of any semiconductor saturable absorber mirror (SESAM) modelocked laser operated in air to date, to the best of our knowledge. This result paves the way to a novel approach for nonlinearity management in high-power lasers.

https://doi.org/10.1364/OPTICA.5.001603

Ultrafast laser technologies are a crucial tool for a wide variety of applications ranging from science, such as time-resolved studies and XUV generation, to industry, for instance, in high-precision material processing. During the last decade, high-power sources based on Yb-doped gain materials, shaped in the thin-disk [1], fiber [2], and slab geometry [3] have had an impressive development, leading to ultrafast amplifier systems exceeding the kW-level average power milestone. Using thin-disk laser (TDL) technology, oscillators delivering multi-100-W average power and tens-of-μJ pulse energy at MHz repetition rate have been demonstrated [4–6]. This approach enables to use a table-top and comparatively cost-effective TDL oscillator as an ultrafast high-power laser source. Hence, TDL oscillators, due to their excellent beam quality and low-noise properties [7], are a highly attractive alternative to multi-stage amplifier systems composed of a low-power oscillator, pulse stretcher, amplification stages, and pulse compressor [2,8]. In fact, TDL oscillators are being used for extra- and intra-cavity XUV generation and high-power frequency conversion to the mid-IR, and are potential sources for high-power THz generation [9].

A significant challenge in these TDL oscillators is the high intracavity peak power, which can exceed 100 MW. At such peak powers, the phase accumulated because of the nonlinear refractive index of the intracavity air represents a major contribution to the overall self-phase modulation (SPM). Since the modelocking process relies on soliton pulse formation, which requires a balance between group-delay dispersion (GDD) and SPM [10], this very large amount of SPM ultimately hinders pulse formation. Different methods have been developed so far to overcome this challenge. One is to compensate this large SPM with a corresponding amount of GDD obtained through dispersive mirrors. This creates a tradeoff between the amount of GDD in the cavity and the output pulse energy of the laser ("Standard TDL" in Fig. 1). However, dispersive mirrors have substantially worse thermal behavior compared to Bragg mirrors, making it very challenging to add a large number of them in a high-power oscillator [8,11]. A different approach consists of operating the oscillator in vacuum or helium environment so that the air contribution to the SPM is almost removed ("Vacuum/He TDL" in Fig. 1) [8]. This approach led to the record results in average power and pulse energy. However, the advantages in performance offered by operation of the TDL in vacuum are offset by the significantly increased cost and complexity of such a system. For many scientific and industrial applications, a simpler solution would be required.

Here, we present a new and much simpler technique to cancel the intracavity SPM picked up in air by exploiting cascaded quadratic nonlinearities (CQN) [12]. In CQN, a second-harmonic-generation (SHG) crystal yields an effective nonlinear refractive index that is tunable in magnitude and sign. CQN have been successfully employed for modelocking of lasers in both the positive and negative dispersion regimes [13–17], pulse compression [18,19], for nonlinear-mirror-type modelocking schemes in TDLs [20,21], and in regenerative amplifiers [22]. Here, we introduce a CQN crystal inside the laser cavity in a phase-mismatched, low-loss configuration. This allows us to cancel up to 80% of the total SPM of air. We balance the remaining SPM through just five dispersive mirrors, enabling soliton pulse formation. We obtain 210-W average power at 780-fs pulse duration, 10.96-MHz repetition rate, and 19.2-μJ pulse energy using $-16,800\ \text{fs}^2$ of GDD ("This result" in Fig. 1). This result

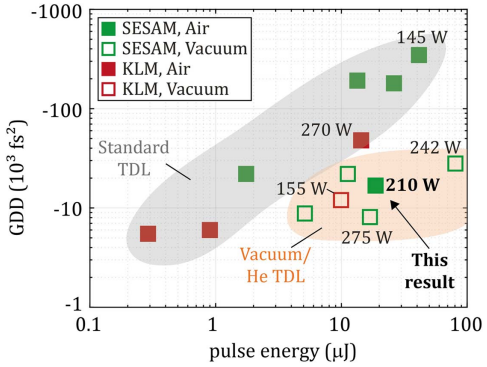

Fig. 1. Overview of the GDD used in TDLs with respect to their output pulse energy. Our result, due to the use of cascaded $\chi^{(2)}$ nonlinearities, overcomes the tradeoff in GDD versus pulse energy typical of standard TDL, lying in a region previously accessible only through expensive vacuum systems. For the non-labeled results, the average output power is below 100 W. All references can be found in Supplement 1.

represents the highest output power of any semiconductor saturable absorber mirror (SESAM) modelocked oscillator operated in air. In the previous record of 145 W [23], −346, 500 fs^2 of round-trip GDD were used. Kerr-lens modelocking (KLM) can require a lower amount of negative GDD for pulse formation (Fig. 1). However, SESAM modelocking is highly advantageous in terms of robust modelocking, since pulse formation is decoupled from cavity stability. Our oscillator also delivers more pulse energy than any KLM oscillator to date, where the record is 14 μJ [6], and more than four times average power compared to previous lasers involving CQN [20].

In our laser experiment we use a 100-μm-thick, 10-at.% doped Yb:YAG disk contacted on diamond (TRUMPF), mounted in a 36-pass head, and pumped at 940 nm with a 4.4-mm-diameter pump spot. We designed a cavity including three reflections on the disk gain medium. Thus, we could use an output coupler (OC) with a comparatively large $T_{OC} = 40\%$ transmission and hence limit the intracavity power. A large OC rate is beneficial in two ways: it reduces the amount of SPM picked up in the intracavity air thus mitigating the requirement of negative GDD, and it decreases the stress on the intracavity components. The folded multi-pass cavity arrangement leads to a lower repetition rate and thus higher pulse energy while keeping a compact footprint (Fig. 2). We introduced a thin-film polarizer (TFP) in the cavity to fix the polarization of the laser.

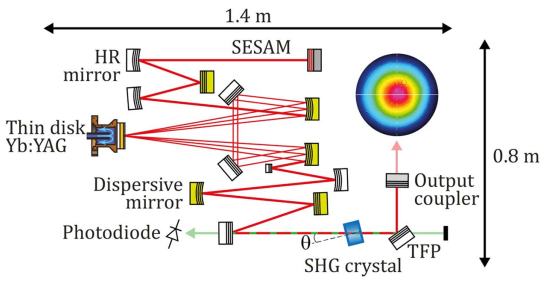

Fig. 2. Schematic of the compact laser cavity including multiple bounces on the disk. The photodiode, through a band-pass green filter, measures the green leakage of a HR mirror. The presented beam profile is obtained in modelocked operation at 210 W output power.

In order to modelock the oscillator, we used an in-house grown SESAM as an end mirror, where the beam radius is ≈850 μm. The SESAM consists of a distributed AlAs/GaAs Bragg reflector grown at 580°C and three InGaAs quantum wells as absorber grown at 280°C in an antiresonant configuration [24,25]. We measured our SESAM to have a saturation fluence $F_{sat} = 50$ μJ/cm^2, a modulation depth $\Delta R = 2.7\%$, and non-saturable losses $\Delta R_{ns} = 0.35\%$ [26]. The SESAM was contacted by TRUMPF on a polished copper heatsink (cold radius of curvature >500 m [25]).

We use only five Gires–Tournois interferometer (GTI)-type dispersive mirrors, yielding a total GDD of $D = -16,800$ fs^2 per round trip. Achieving 210-W output power with 780-fs pulses without CQN would require ≈5 times more negative GDD. Thus, the use of CQN critically helps the balance between SPM and GDD. CQN offer a large effective nonlinear refractive index contribution $n_{2,CQN}$, which depends on the second-order nonlinear coefficient d_{eff} and the phase mismatch $\Delta k = k_{SH} - 2k_{FW}$, where SH stands for second harmonic and FW for fundamental wave. This $n_{2,CQN}$ can be tuned in sign and magnitude via Δk [12]. In this laser experiment, we exploit a negative $n_{2,CQN}$ from a SHG crystal in order to pick up a negative nonlinear phase shift, which counteracts the positive one picked up in air. A potential drawback of this technique is the loss caused by the SH generated in the cascading processes, since the SH light is not resonant in the laser cavity. The SHG efficiency scales with the peak intensity; hence, it represents an inverse saturable loss. On the other hand, if such losses are small compared to the modulation depth of the SESAM ΔR, this property can stabilize the modelocking process [16,27]. In order to minimize the second-harmonic losses, we operate the crystal near the SHG minima, which correspond to $\Delta kL \approx 2\pi n_{min}$, where L is the length of the crystal and n_{min} is an integer. Experimentally, we monitor the SHG losses measuring the power of a cavity green leakage ("Photodiode" in Fig. 2) and adjust the crystal's tilt angle θ through a piezo-controlled mount. In this way, we can operate the crystal in the SHG minima.

To quantify the losses and the phase shift introduced by the CQN device, let us consider a pulse with peak intensity I_{pk}, progressing through the SHG crystal. We call the phase shift introduced for the peak of the pulse $B_{CQN,sp}$ and the efficiency of the SHG process $\eta_{CQN,sp}$:

$$B_{CQN,sp} \approx -\xi L I_{pk}/\Delta k, \tag{1a}$$

$$\eta_{CQN,sp} \approx 0.83\xi(\delta L)^2 I_{pk}/(\Delta k \tau_p)^2, \tag{1b}$$

where we define a group-velocity mismatch parameter $\delta = 1/v_{g,SH} - 1/v_{g,FW}$, $\xi = 2[\omega_{FW} d_{eff}]^2/[\varepsilon_0 c^3 (n_{FW})^2 n_{SH}]$, and τ_p is the full-width-at-half-maximum (FWHM) duration of the pulse, assuming a sech^2 shape. These equations assume the cascading regime, where the phase mismatch is large and the transfer of energy from the fundamental to the second harmonic is small. The phase shift presented in Eq. (1a) has a well-known expression in literature [28]. We obtain Eq. (1b) in the supplementary material assuming a short crystal fulfilling $\tau_p > 2\delta L$, together with a large enough Δk, and operation in a SHG minimum (i.e., $\Delta kL = 2\pi n_{min}$). In this short-crystal regime, the phase mismatch $\Delta k(\lambda)$ is close to $2\pi n_{min}$ across the whole pulse spectrum, allowing for very low SHG losses for the

intracavity pulse. Hence, the ratio between nonlinear phase shift [Eq. (1a)] and nonlinear losses [Eq. (1b)] is lower than in the long-crystal limit ($\tau_p \ll \delta L$) [13]. Additionally, short crystals are beneficial in high-power applications in order to minimize thermal lensing.

The free parameters in the design of the CQN device are the crystal length L, the intensity on the crystal I_{pk}, adjustable through the laser spot size on the SHG crystal, and the phase mismatch Δk. The goal is to get a large amount of negative phase shift and as little as possible SHG losses, i.e., to maximize $B_{\mathrm{CQN,sp}}/\eta_{\mathrm{CQN,sp}} \sim \Delta k/L$. Thus, our formulas suggest to use short crystals operated at large phase-mismatch angles. We employed an AR-coated type-I LBO crystal (Cristal Laser) with a length $L = 5$ mm, in a position where the $1/e^2$ beam radius is ≈850 μm. In this way, we have a peak intensity on the crystal below 5 GW/cm^2.

We next consider the balance of the different sources contributing to the cavity SPM. The total phase shift $B_{\mathrm{CQN,rt}}$ and losses $\eta_{\mathrm{CQN,rt}}$ per round trip due to the SHG crystal are obtained multiplying the single-pass values [Eqs. (1a) and (1b)] for $(1 + R_{\mathrm{OC}})$ where $R_{\mathrm{OC}} = 60\%$ is the reflectivity of the OC. A convenient way to express the phase shift is to introduce the SPM coefficient $\gamma = B/P_{\mathrm{pk,IC}}$, where $P_{\mathrm{pk,IC}}$ is the intracavity peak power immediately before the OC. Regarding the air, we integrate the peak intensity in a cavity round trip to obtain the total SPM, denoted $B_{\mathrm{air,rt}}$ (Supplement 1), and we obtain $\gamma_{\mathrm{air}} \approx 10.6$ mrad/MW. In Fig. 3, we plot the expected losses $\eta_{\mathrm{CQN,rt}}$ and the SPM coefficients γ_{CQN} for the CQN device, according to our analytical model (green) and a numerical simulation (blue). We use $d_{\mathrm{eff}} = 0.83$ pm/V for LBO [29]. We obtained the numerical solution by directly solving the pulsed coupled-wave equations for the laser parameters at the maximum output power ($\tau_p = 780$ fs, $P_{\mathrm{pk,IC}} = 54$ MW). For the intrinsic nonlinear refractive index of the LBO, we use 2×10^{-16} cm^2/W [30]. The analytical model accurately predicts the SHG losses in the minima and the phase shift. The positive contribution to the phase shift from the crystal's intrinsic n_2 leads to a slightly less negative SPM coefficient γ_{CQN} in the numerical model compared to the analytical solution, since this term is not included in the latter. The other sources of SPM, e.g., the disk, contribute only by few percent and so have been neglected.

Femtosecond SESAM-modelocked lasers rely on soliton pulse formation. In this regime of SESAM modelocking, pulse duration and intracavity pulse energy $E_{\mathrm{IC}} = E_{\mathrm{out}}/T_{\mathrm{OC}}$ depend mostly on the GDD versus SPM balance and only marginally on the parameters of the saturable absorber [10]. Their relation is governed by the so-called soliton formula, $\tau_p \approx 1.76(2|D|)/(\gamma^{\mathrm{avg}} E_{\mathrm{IC}})$, where $\gamma^{\mathrm{avg}} = 3/4\ \gamma$ takes into account the effective phase shift for a pulse with a Gaussian spatial profile compared to the phase shift for the peak of the pulse [16,31]. By tuning the phase mismatch Δk, we can adjust the net SPM coefficient γ [Fig. 3(b)]. Thanks to the straight-forward tunability of Δk by adapting the crystal's tilt during live laser operation, we obtain the shortest pulse duration for several values of the output power (cfr. Fig. 4 and Table 1). In contrast, a standard TDL, having a fixed amount of GDD and SPM, operates only over a fixed power range and has the shortest pulses only at the maximum output power. In Fig. 4 we present the laser output power versus pump power for three phase-matching configurations. The blue and red curves are obtained operating the SHG crystal, respectively, in the fourth ($\Delta kL \approx 8\pi$) and third ($\Delta kL \approx 6\pi$) SHG minimum. The slope in yellow is obtained starting from the third SHG minimum and gradually decreasing the Δk as the pump power is increased, in order to reduce the net SPM coefficient γ. Like this, we keep the pulse duration equal to the minimum achievable for our laser, but at increased output power. At the maximum output power (210 W, 780 fs), we measured a SHG efficiency ≈1.8 times the one we had in the third SHG minimum. This suggests a shift in ΔkL from the third SHG minimum of $\approx -0.2\pi$, i.e., $\Delta kL \approx 5.8\pi$. For this value of ΔkL, we have $n_{2,\mathrm{CQN}} \approx -2.1 \times 10^{-15}$ cm^2/W [28].

Next, in Table 1, we quantify the SPM cancellation effect occurring in the laser for several operating points. Except for the point at 210-W output power, we experimentally optimized

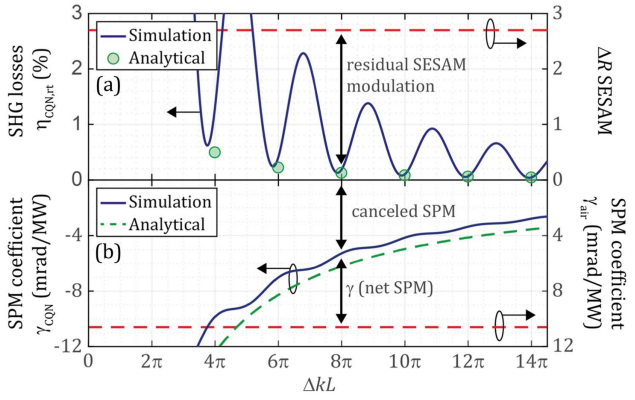

Fig. 3. Round-trip SHG losses (a) and SPM cancellation (b) due to the CQN device. By operating the crystal in a SHG minimum, few-0.1% losses can be obtained while canceling most of the SPM from air.

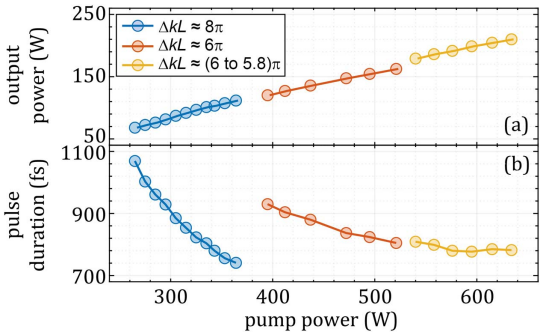

Fig. 4. Laser slopes: output power (a) and pulse duration (b) as a function of the pump power. Different colors refer to different phase mismatch values Δk of the SHG crystal.

Table 1. Laser Parameters for $\tau_p \approx 800$ fs[a]

n_{min}	ΔkL	P_{out} (W)	τ_p (fs)	$\gamma_{\mathrm{soliton}}$	$\gamma_{\mathrm{soliton}} - \gamma_{\mathrm{air}}$ (mrad/MW)	γ_{CQN}	$\lvert\frac{\gamma_{\mathrm{CQN}}}{\gamma_{\mathrm{air}}}\rvert$
	≈5.8π	210	782	2.1	−8.5	−8.6	81%
3	≈6π	162	805	2.6	−8.0	−8.3	78%
4	≈8π	112	741	4.2	−6.4	−6.2	59%
5	≈10π	85	749	5.5	−5.1	−5.0	47%
6	≈12π	72	782	6.2	−4.4	−4.1	39%
7	≈14π	61	865	6.6	−4.0	−3.6	33%

[a] $\gamma_{\mathrm{soliton}}$ is obtained from the soliton formula $\gamma_{\mathrm{air}} = 10.6$ mrad/MW, and γ_{CQN} is the expected negative SPM coefficient from the CQN device. The last column represents the fraction of SPM from air canceled by CQN.

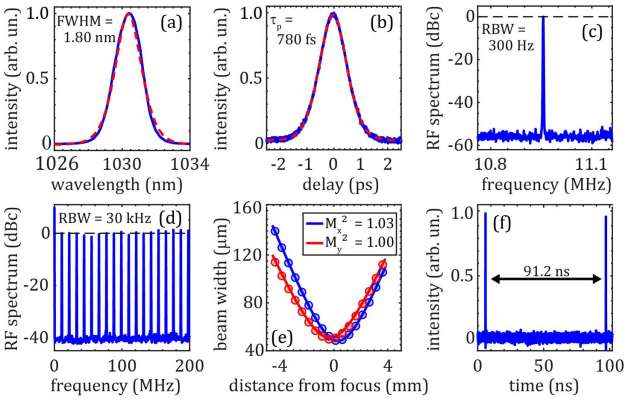

Fig. 5. Laser diagnostics at the maximum output power (210 W, 780 fs, 19 μJ). (a) Optical spectrum; (b) intensity autocorrelator; (c)–(d) RF spectra with 0-dBc marked by black dashed line; (e) M^2 measurement; (f) sampling oscilloscope trace. RBW, resolution bandwidth. The autocorrelation trace and the optical spectrum are fitted with a sech^2 function (red dashed line). The $1/e^2$ beam width is calculated using the second momentum ($D4\sigma$).

the crystal's phase mismatch in order to operate in the SHG minima, i.e., $\Delta kL \approx 2\pi n_{\mathrm{min}}$. For the point at 210-W output power, we slightly detuned the phase mismatch from the third SHG minimum, as described above. The soliton formula together with the measured laser characteristics yields a prediction for the total round-trip SPM coefficient, denoted $\gamma_{\mathrm{soliton}}$. Two contributing terms to this SPM coefficient are the intracavity air γ_{air}, and the CQN crystal γ_{CQN}, which we calculate according to $\gamma_{\mathrm{air}} = B_{\mathrm{air,rt}}/P_{\mathrm{pk,IC}}$ and $\gamma_{\mathrm{CQN}} = B_{\mathrm{CQN,rt}}/P_{\mathrm{pk,IC}}$, respectively. We expect $\gamma_{\mathrm{soliton}} = \gamma_{\mathrm{air}} + \gamma_{\mathrm{CQN}}$. In Table 1, we compare $\gamma_{\mathrm{soliton}} - \gamma_{\mathrm{air}}$ to γ_{CQN}, to show that the laser characteristics are in good agreement with this equation. The last column of the table presents the percentage of the SPM picked up in air canceled by the CQN device. It ranges from ≈30% to ≈80% showing the great flexibility of this technique.

In Fig. 5 we present the laser diagnostics at the maximum output power, which show a single-pulse stable modelocked operation. We ensure single-pulsed operation by scanning the autocorrelator delay up to 60 ps and acquiring a sampling oscilloscope trace with a 45-GHz photodiode [Fig. 5(f)]. We obtain diffraction-limited beam quality ($M^2 < 1.05$) in all configurations. In the presented laser, the output power was limited by the pump intensity on the disk, already close to the safety limit of 5 kW/cm^2, and the fluence on the SESAM, which was already operated slightly into the rollover.

In conclusion, we demonstrated a novel concept to cancel the SPM picked up in air in the context of high-power ultrafast oscillators. This allowed us to obtain laser performance in line with best-in-class TDLs using, instead of a complex vacuum system, an inexpensive and easy-to-set-up nonlinear crystal. Next to SESAM-modelocked TDL, this technique can be applied to high-power KLM oscillators. Additionally, we prove here that self-defocusing nonlinearities can be used at unprecedented power levels of up to 500 W intracavity power, hence offering a new toolset for high-average-power lasers.

Funding. Schweizerischer Nationalfonds zur Förderung der Wissenschaftlichen Forschung (SNF) (200020_172644).

See Supplement 1 for supporting content.

REFERENCES

1. T. Nubbemeyer, M. Kaumanns, M. Ueffing, M. Gorjan, A. Alismail, H. Fattahi, J. Brons, O. Pronin, H. G. Barros, Z. Major, T. Metzger, D. Sutter, and F. Krausz, Opt. Lett. **42**, 1381 (2017).
2. M. Müller, M. Kienel, A. Klenke, T. Gottschall, E. Shestaev, M. Plötner, J. Limpert, and A. Tünnermann, Opt. Lett. **41**, 3439 (2016).
3. P. Russbueldt, D. Hoffmann, M. Hoefer, J. Loehring, J. Luttmann, A. Meissner, J. Weitenberg, M. Traub, T. Sartorius, D. Esser, R. Wester, P. Loosen, and R. Poprawe, IEEE J. Sel. Top. Quantum Electron. **21**, 3100117 (2015).
4. C. J. Saraceno, F. Emaury, O. H. Heckl, C. R. E. Baer, M. Hoffmann, C. Schriber, M. Golling, T. Südmeyer, and U. Keller, Opt. Express **20**, 23535 (2012).
5. C. J. Saraceno, F. Emaury, C. Schriber, M. Hoffmann, M. Golling, T. Südmeyer, and U. Keller, Opt. Lett. **39**, 9 (2014).
6. J. Brons, V. Pervak, E. Fedulova, D. Bauer, D. Sutter, V. Kalashnikov, A. Apolonskiy, O. Pronin, and F. Krausz, Opt. Lett. **39**, 6442 (2014).
7. F. Emaury, A. Diebold, C. J. Saraceno, and U. Keller, Optica **2**, 980 (2015).
8. C. J. Saraceno, F. Emaury, C. Schriber, A. Diebold, M. Hoffmann, M. Golling, T. Südmeyer, and U. Keller, IEEE J. Sel. Top. Quantum Electron. **21**, 1100318 (2015).
9. C. J. Saraceno, J. Opt. **20**, 044010 (2018).
10. F. X. Kärtner, I. D. Jung, and U. Keller, IEEE J. Sel. Top. Quantum **2**, 540 (1996).
11. O. Razskazovskaya, T. T. Luu, M. Trubetskov, E. Goulielmakis, and V. Pervak, Optica **2**, 803 (2015).
12. F. Wise, L. Qian, and X. Liu, J. Nonlinear Opt. Phys. Mater. **11**, 317 (2002).
13. C. R. Phillips, A. S. Mayer, A. Klenner, and U. Keller, Opt. Express **22**, 6060 (2014).
14. L. J. Qian, X. Liu, and F. W. Wise, Opt. Lett. **24**, 166 (1999).
15. G. Cerullo, S. De Silvestri, A. Monguzzi, D. Segala, and V. Magni, Opt. Lett. **20**, 746 (1995).
16. A. S. Mayer, C. R. Phillips, and U. Keller, Nat. Commun. **8**, 1673 (2017).
17. H. Iliev, D. Chuchumishev, I. Buchvarov, and V. Petrov, Opt. Express **18**, 5754 (2010).
18. A. L. Viotti, R. Lindberg, A. Zukauskas, R. Budriunas, D. Kucinskas, T. Stanislauskas, F. Laurell, and V. Pasiskevicius, Optica **5**, 711 (2018).
19. M. Bache, O. Bang, W. Krolikowski, J. Moses, and F. W. Wise, Opt. Express **16**, 3273 (2008).
20. B. Borchers, C. Schaefer, C. Fries, M. Larionov, and R. Knappe, in *Advanced Solid State Lasers* (OSA, 2015), paper ATh4A.9.
21. F. Saltarelli, A. Diebold, I. J. Graumann, C. R. Phillips, and U. Keller, Opt. Express **25**, 23254 (2017).
22. C. Dorrer, R. G. Roides, J. Bromage, and J. D. Zuegel, Opt. Lett. **39**, 4466 (2014).
23. D. Bauer, I. Zawischa, D. H. Sutter, A. Killi, and T. Dekorsy, Opt. Express **20**, 9698 (2012).
24. C. J. Saraceno, C. Schriber, M. Mangold, M. Hoffmann, O. H. Heckl, C. R. E. Baer, M. Golling, T. Südmeyer, and U. Keller, IEEE J. Sel. Top. Quantum Electron. **18**, 29 (2012).
25. A. Diebold, T. Zengerle, C. G. E. Alfieri, C. Schriber, F. Emaury, M. Mangold, M. Hoffmann, C. J. Saraceno, M. Golling, D. Follman, G. D. Cole, M. Aspelmeyer, T. Südmeyer, and U. Keller, Opt. Express **24**, 10512 (2016).
26. D. J. H. C. Maas, B. Rudin, A.-R. Bellancourt, D. Iwaniuk, S. V. Marchese, T. Südmeyer, and U. Keller, Opt. Express **16**, 7571 (2008).
27. T. R. Schibli, E. R. Thoen, F. X. Kärtner, and E. P. Ippen, Appl. Phys. B **70**, S41 (2000).
28. G. I. Stegeman, D. J. Hagan, and L. Torner, Opt. Quantum Electron. **28**, 1691 (1996).
29. S. P. Velsko, M. Webb, L. Davis, and C. Huang, IEEE J. Quantum Electron. **27**, 2182 (1991).
30. H. P. Li, C. H. Kam, Y. L. Lam, and W. Ji, Opt. Mater. **15**, 237 (2001).
31. J. Herrmann, J. Opt. Soc. Am. B **11**, 498 (1994).